

# Hydrogen-induced ferromagnetism in ZnO single crystals investigated by Magnetotransport

M. Khalid\* and P. Esquinazi

*Division of Superconductivity and Magnetism, Institute for Experimental Physics II,  
University of Leipzig, D-04103 Leipzig, Germany*

(Dated: June 24, 2018)

We investigated the electrical and magnetic properties of low-energy hydrogen-implanted ZnO single crystals with hydrogen concentrations up to  $\sim 3$  at.% in the first 20 nm surface layer between 10 K and 300 K. All samples showed clear ferromagnetic hysteresis loops at 300 K with a saturation magnetization up to  $\simeq 4$  emu/g. The measured anomalous Hall effect agrees with the hysteresis loops measured by superconducting quantum interferometer device magnetometry. All the H-treated ZnO crystals exhibited a negative magnetoresistance up to the room temperature. The relative magnitude of the anisotropic magnetoresistance reaches 0.4 % at 250 K and 2 % at 10 K, exhibiting an anomalous, non-monotonous behavior and a change of sign below 100 K. All the experimental data indicate that hydrogen atoms alone in a few percent range trigger a magnetic order in a ZnO crystalline state. Hydrogen implantation turns out to be a simpler and effective method to generate a magnetic order in ZnO, which provides interesting possibilities for future applications due to the strong reduction of the electrical resistance.

PACS numbers: 75.30.Cr, 75.50.Pp, 75.60.Ej

## I. INTRODUCTION

Defect-induced magnetism (DIM) appears to be a general phenomenon observed in nominally non-magnetic solids starting from the archetype graphite[1, 2] to several oxides like ZnO, pure or doped with non-magnetic elements [3–8], HfO<sub>2</sub> [9], TiO<sub>2</sub> [10, 11], SrTiO<sub>3</sub> [8, 12], SrO:N [13] as well as Si-based samples[14], to mention only a few examples from a large number being reported nowadays (for recent reviews on this subject see Refs. 15–18). Experimental facts demonstrate that defects, like vacancies, without or with the presence of non-magnetic ad-atoms, play a main role in triggering magnetic order in these systems. Recently, room temperature ferromagnetism was reported in Cu-doped ZnO films, investigated by soft x-ray magnetic circular dichroism [19]. The results of this study strengthens the existence of the DIM phenomenon in general and in ZnO in particular.

ZnO is a wide band gap semiconductor, which crystallizes in the hexagonal wurtzite, zincblende and rocksalt structures. However, hexagonal wurtzite is the most intensively studied crystal structure of ZnO because of its potential applications in the field of spintronics, transparent electronics, piezoelectricity, optoelectronics, etc. Hydrogen is one of the most abundant and unavoidable impurities in ZnO. The presence of hydrogen can influence the electrical and the magnetic properties of ZnO. The role of hydrogen in enhancing the ferromagnetism in 3d-transition metal-doped ZnO was recently studied experimentally [20] and theoretically[21]. On the other side there are theoretical studies reporting on the possibility of room temperature ferromagnetism due to hydrogen

adsorption at the surface of ZnO[22, 23]. We note however that there is a lack of experimental and theoretical studies on the possibility of hydrogen-induced magnetic order inside the crystalline structure of pure ZnO.

In this work we are interested on DIM in ZnO crystals triggered through the implantation of hydrogen at low energies and its influence on the magnetotransport. We report on a detailed experimental study that demonstrates how the intentional doping of hydrogen in the percent range and at low-enough energies influences substantially the electrical, magnetic and magnetotransport properties of ZnO single crystals. In particular, we show in this report a hydrogen-induced anisotropic magnetoresistance (AMR) as well as the anomalous Hall effect (AHE) in H-ZnO single crystals. Therefore, the existence of hydrogen-induced ferromagnetism in H-ZnO samples is supported not only by the usual magnetization data taken with a superconducting quantum interference device (SQUID)[24] but also from magnetotransport measurements.

## II. EXPERIMENTAL DETAILS

Hydrothermally grown ZnO (0001) single crystals of dimensions  $(6 \times 6 \times 0.5)$  mm<sup>3</sup> with both sides polished were supplied by CrysTec GmbH. The ZnO samples were exposed to remote hydrogen dc plasma for different time intervals in a parallel-plate system. The voltage difference between the two plates was kept at 1 kV. The samples were mounted on a heater block held at a fixed temperature of 400 °C and they were placed  $\sim 100$  mm down stream from the plasma with a bias voltage of  $\sim -330$  V. A bias current of  $\sim 50$   $\mu$ A was measured during the plasma treatment. The pressure in the chamber during the process was maintained around 1 mbar. Three samples H-1,

---

\*Electronic address: m.khalid@physik.uni-leipzig.de

H-2 and H-3 for time intervals 30, 60 and 90 min, respectively, were treated in the H-plasma chamber. The implantation depth (for the chosen energy) as well as for the concentration characterization analysis (see below) were estimated using SRIM[25]. From this Monte Carlo simulation program we estimate a penetration depth of 20 nm for the implanted hydrogen atoms. As experimentally shown in Ref.[24] the main ferromagnetic signal comes from this near surface region, in agreement with the estimates.

Nuclear reaction analysis (NRA) was used to determine the hydrogen concentration in ZnO crystals before and after hydrogen plasma treatment [26]. The NRA has a depth resolution of  $\sim 5$  nm with an average error in the concentration of 0.02%. The hydrogen concentration in ZnO crystals measured by NRA before and after remote hydrogen treatment was found to be  $0.14 \pm 0.03$  and  $0.64 \pm 0.07$  at.% in the first 200 nm from the surface, respectively[27]. From this concentration analysis we conclude that the first 20 nm near surface region should have a hydrogen concentration of the order of  $\sim 3$  at.% for sample H-3. The hydrogen concentrations for samples H-1 and H-2 are  $\sim 1$  at.% and  $\sim 1.8$  at.%, respectively.

We performed Particle Induced X-ray Emission (PIXE) measurements to analyze the concentration of magnetic impurities in the H-ZnO samples. There was no significant difference in the Fe concentration ( $< 60$  ppm) before and after H-plasma treatment.

The magnetization of the ZnO single crystals before and after the plasma treatment was determined with a SQUID. The magnetotransport measurements were performed in an Oxford cryostat with a magnetic field up to 8 T and a rotating sample holder allowing us to measure the resistance at different angles between magnetic field and the input current. The electrical contacts on the samples were prepared using silver paste in a Van der Pauw configuration. The  $I/V$  characteristics were measured to check for deviations from the ohmic behavior. All the transport data presented in this paper were taken in a linear, ohmic regime. The resistance was measured with an ac resistance bridge with a relative resolution of 0.01%.

### III. RESULTS AND DISCUSSION

#### A. Magnetization Measurements

Figure 1(a) shows the magnetic moment after subtraction of the linear diamagnetic contribution vs. applied field measured at 5 K for all three samples with the SQUID. This signal is composed by two contributions. The main one is paramagnetic and follows the usual Brillouin or Langevin function. If one subtracts it from the data a small ferromagnetic contribution still remains, as can be seen in the inset of Figure 1(a) for sample H-3.

At 300 K the paramagnetic contribution is negligible

and the measured signal is given by the addition of the diamagnetic plus the ferromagnetic one of the near surface region. After subtraction of the diamagnetic contribution the magnetization coming from the ferromagnetic part was calculated assuming a ferromagnetic mass homogeneously located at the first 20 nm near surface region[24], see Fig. 1(b). We see that the magnetization increases with H-implantation as reported in Ref. 24 and also decreasing temperature, compare the results of sample H-3 in Fig. 1(b) with those in the inset of Fig. 1(a). The ferromagnetic magnetization per total volume of a virgin, untreated ZnO crystal of the same type as used here, is of the order of  $10^{-4}$  emu/g[8]. For comparison and taking into account that a similar near surface region in nonmagnetic oxide crystals could be the source for the ferromagnetic signals[8], the untreated ZnO crystal would have a saturation ferromagnetic magnetization half of that of sample H-1.

All samples exhibit a coercivity of 18-20 mT at room temperature. The saturation magnetization increases by increasing the H-concentration and reaches  $\simeq 4$  emu/g for sample H-3. The ferromagnetic magnetization at 5 K increases by  $\sim 50\%$  of its value at room temperature (see inset in Fig. 1(a)). From the measurement of the ferromagnetic remanent magnetic moment we estimate a Curie temperature of  $450 \pm 25$  K [24].

Recently, N. Sanchez et al.[22] have theoretically shown that atomic hydrogen adsorbed on the Zn-ZnO (0001) surface can form strong H-Zn bonds and lead to a metallic surface with a net magnetic moment of  $0.5 \mu_B$  per H-atom. The obtained magnetization values indicate that our H-3 sample, for example, would have a net magnetic moment of  $0.2 \mu_B$  per hydrogen atom. This estimate is obtained taking into account the amount of H implanted. The difference between the two estimates may indicate that the assumed ferromagnetic mass is larger than the true one. This appears plausible because the hydrogen atoms are not necessarily homogeneously distributed inside its penetration depth. We believe that in the first 20 nm depth we have regions where the magnetic order is less developed and therefore one tends to overestimate the ferromagnetic mass. This picture of a rather inhomogeneous mixture of magnetic and non-magnetic regions is of importance to interpret the transport data, as we shall discuss below.

#### B. Resistivity Measurements

We measured the temperature dependence of the resistance of the three H-ZnO samples from 10 K to 270 K, see Fig. 2. The resistance decreases increasing H-concentration, therefore it is reasonable to assume that the resistivity of the implanted part is much smaller than the resistivity from the rest of the single crystal, as has been already reported [28]. This assumption is supported by the direct comparison of the estimated values of the resistivity – assuming conduction within the 20 nm im-

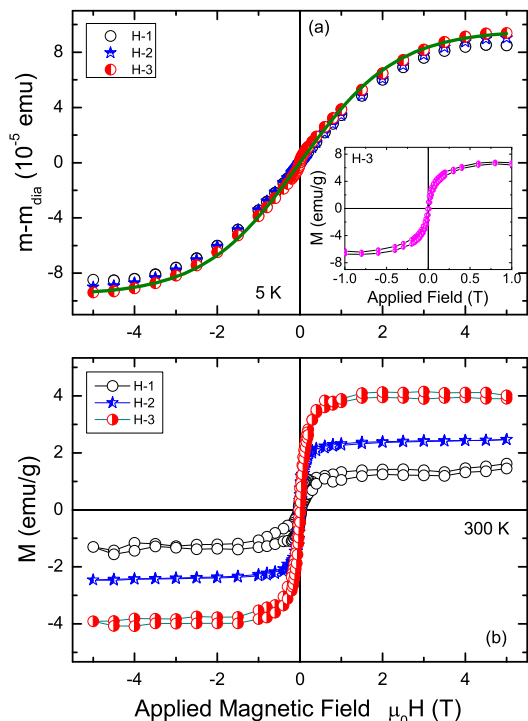


FIG. 1: (a) Magnetic moment of the three H-ZnO crystals as a function of magnetic field at 5 K. The inset shows a ferromagnetic contribution which is left after subtracting a paramagnetic one obtained by using the Langevin function. (b) Ferromagnetic magnetization of the same crystals at 300 K assuming a homogeneously distributed ferromagnetic mass at the first 20 nm near surface region[24]. A diamagnetic slope was subtracted from the data. Note that the magnetization of H-ZnO crystals increases with H-concentration.

planted thickness, right  $y$ -axis in Fig. 2 – with the resistivity of the virgin ZnO single crystal, which is already at room temperature several orders of magnitude larger[29].

Before discussing in detail the observed behavior of the resistivity, we would like to describe shortly what is known about the hydrogen contribution to the formation and/or modification of the electronic band structure in ZnO. Hydrogen forms shallow donor states in bulk ZnO and is regarded as a source for n-type conductivity. These shallow donor states are formed approximately 30-60 meV below the conduction band. Upon doping level the donor energy states can be dispersed into an impurity band because of the Coulomb fields arising from the compensating acceptors and ionized donors[30]. This impurity band could further split into two bands, i.e. a lower band I and an upper band I<sup>-</sup>, which are formed with single charged donors and neutral donors, respectively[31, 32].

As we have already noted in section 3A, we assume that the implanted H<sup>+</sup>-ions are not homogeneously distributed in H-ZnO samples. Then, we may have

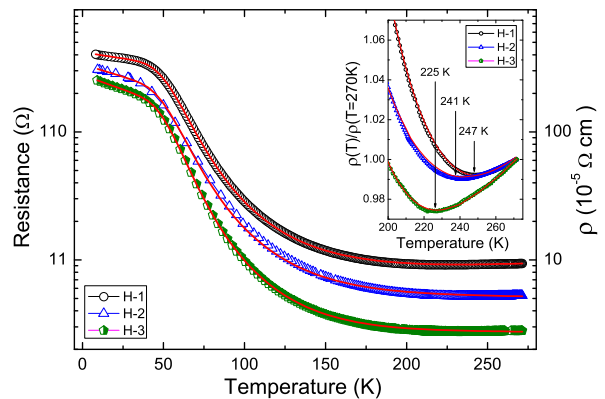


FIG. 2: Resistance of the three H-ZnO samples as a function of temperature at a zero applied field. At the right  $y$ -axis we show the resistivity estimated taken into account 20 nm implanted thickness of the single crystal. The inset blows out the high temperature part where the resistance shows a qualitative change in its temperature dependence. The observed minimum shifts to the low temperatures by increasing the hydrogen concentration. The red solid lines show the fits of the data to Eq. (2). The obtained values for  $R_1$ ,  $R_2$  and  $R_3$  are (0.022, 0.014, 0.015)  $\Omega$ , (0.587, 0.612, 0.365)  $\Omega$  and (197, 143, 169)  $\Omega$  for samples (H-1, H-2, H-3), respectively. The rest resistance for all samples is  $R_0 \leq 10^{-6} \Omega$ .

hydrogen-rich metallic regions with resistance  $R_m(T) = R_0 + R_1 T$ , embedded in a doped semiconducting matrix with resistance  $R_s(T) = R_2 \exp(\Delta E/2k_B T)$  ( $k_B$  is the Boltzmann constant).  $R_0$ ,  $R_1$ ,  $R_2$  are free parameters as well as the activation energy  $\Delta E$  which will be obtained by fitting the experimental data. Note that we consider a linear  $T$  dependence for the metallic part in all the temperature range. The metallic region contributes mainly at high enough temperatures, see inset in Fig. 2, and therefore it is unnecessary to assume a more complicated  $T$ -dependence that may be applicable at temperatures  $T < 100$  K. We consider that these two contributions, the metallic- and semiconducting-like are in series. Due to the implantation distribution curve [24], it is clear that below  $\sim 20$  nm a third intermediate region should exist that contributes with a resistance  $R_h(T)$  in parallel to the other two. The best fits have been achieved by assuming a variable range hopping (VRH)-like mechanism as:

$$R_h = R_3 \exp\left(\frac{E_{nn}}{T}\right)^{1/5}. \quad (1)$$

Where  $R_3$  is a free parameter and  $E_{nn}$  is a hopping energy. The total resistance will be given then by

$$R(T) = \left[ (R_h(T))^{-1} + (R_m(T) + R_s(T))^{-1} \right]^{-1}. \quad (2)$$

One can also take into account a fourth parallel resistance contribution arising from the pure ZnO single

crystal below a  $\sim 100$  nm thick layer. However, the resistance of such pure ZnO crystal at all temperatures is in the range of  $M\Omega$  and therefore its contribution to the total resistance is negligible. The fittings to the data of the three crystals are reasonably good as we can see in Fig. 2. The activation energy obtained from the fittings for the three H-ZnO single crystals is  $60 \pm 2$  meV.

Qualitatively the observed temperature dependence of the resistivity is rather simple to understand. At temperatures below 50 K, the resistance of the semiconducting contribution  $R_s$  is larger than the resistance  $R_h(T)$ , becoming this last the dominant transport mechanism[33] because the thermal energy is not enough to excite the electrons from the upper impurity band  $I^-$  to the conduction band. The hopping energy obtained from the fitting of the experimental data is  $E_{nn} \simeq 3 \pm 0.5$  meV. As the temperature increases the resistance of the H-ZnO samples decreases following a semiconducting behavior with an effective activation energy  $\Delta E \simeq 60$  meV. The larger the hydrogen doping the lower is  $R_m(T)$  and therefore the lower is the temperature of the minimum, see inset in Fig. 2. Although with this simple model we can understand qualitatively the behavior measured in the resistance as a function of temperature and hydrogen concentration, it does not provide us with a clear hint about the regions that contribute to the magnetic signal. If the magnetic order is confined mostly within the first 20 nm surface region[24] we expect then that either the metallic or the semiconducting regions or even an intermediate region between these two and the VRH part, contributes to the ferromagnetic signal. As the semiconducting contribution overwhelms in a wide temperature range the metallic one, it appears plausible that this one may be responsible for the magnetoresistance behavior we have observed in H-ZnO single crystals.

### C. Charge Carriers

We performed Hall measurements in a Van der Pauw configuration in order to obtain the charge carriers density of our H-ZnO samples. Our Hall measurements confirm that the conductivity in H-ZnO single crystals is n-type. We note that the estimated carrier concentration is an effective one obtained using the simplest expression  $n = 1/R_{He}$ , where  $R_H$  is the Hall resistance, assuming that only the sample volume of the first 20 nm H-rich surface layer of the ZnO single crystals contributes. In case electrons and holes would contribute with different densities and scattering rates then the two-band model is necessary to obtain the carrier densities. The use of its equations, however, implies the introduction of free, unknown parameters, like the scattering rates. In order to facilitate the comparison of our data with literature values we prefer to discuss the carrier density from the Hall data stressing that the measurable quantity is  $R_H$ . The temperature dependent of the carrier density  $n_H$  is shown in Fig. 3.

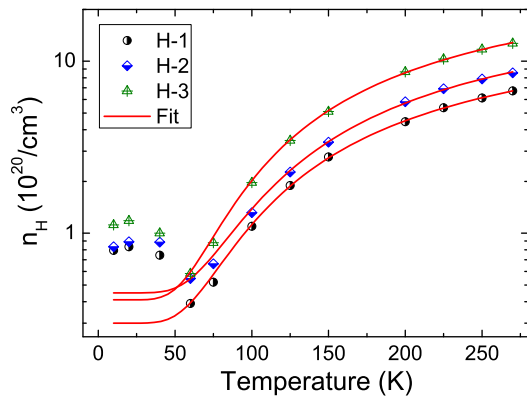


FIG. 3: (a) Carrier density of the three H-ZnO single crystals as a function of temperature. The carrier density shows an anomalous behavior around  $\sim 50$  K. The solid lines are fit to the expression given in Eq.( 3).

The carrier concentration of samples H-1, H-2 and H-3 at room temperature are  $6.72 \times 10^{20} \text{cm}^{-3}$ ,  $8.56 \times 10^{20} \text{cm}^{-3}$  and  $1.27 \times 10^{21} \text{cm}^{-3}$ . These values are comparable to those found in, e.g., Ga-doped ZnO system[34]. Above  $T \sim 50$  K the carrier density increases with temperature following the equation:

$$n_H = a + b \exp\left(\frac{\Delta E}{2k_B T}\right), \quad (3)$$

where  $a, b$  are free parameters. The activation energy obtained from the fits is  $\Delta E = 60 \pm 2$  meV, in agreement to the activation energy values obtained from the resistivity measurements, see Fig. 2. As expected, the carrier concentration increases with hydrogen concentration. The increase in  $n_H$  between the samples agrees roughly with the estimated increase in the hydrogen concentration.

At temperatures  $T \lesssim 50$  K,  $n_H$  increases with a decrease in temperature, see Fig. 3. This is an anomalous behavior that appears to be related to the change of the main contribution to the measured resistance, i.e. from the semiconducting region above 50 K to the VRH one below it, see Fig. 2. In this case it might be that the simple relation to estimate  $n_H(T < 50\text{K})$  from the Hall resistance is not adequate and a more complicated equation for the Hall signal of a material with two contributions in parallel should be used[35]. We note that the anomaly at  $T \sim 50$  K is observed in all the magnetotransport properties we have measured, as we will show in the following sections.

### D. Magnetoresistance Measurements

Apart from the magnetization measurements a further and important way to check for the existence of magnetic order is through the measurement of the magnetotransport properties. Unlike magnetization measurements, magnetotransport properties are much less sensi-

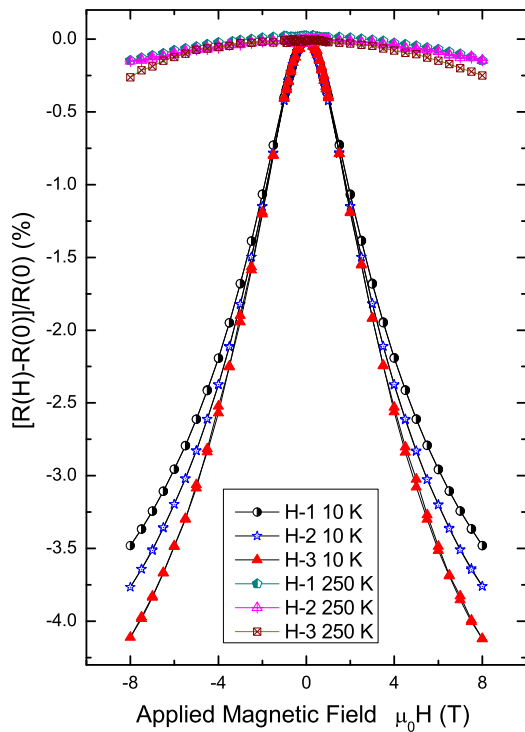


FIG. 4: Magnetoresistance (in percentage) as a function of applied magnetic field at 10 K and 250 K for the three H-ZnO samples. A clear correlation between magnetoresistance and H-concentration is observed. The magnetoresistance increases with H-concentration.

tive to magnetic impurities, in case they remain below  $\sim 0.1\%$ , and in general they reflect intrinsic characteristics of the sample. In this section we discuss the longitudinal magnetoresistance of H-ZnO where the magnetic field is applied parallel to the input current as well as to the sample main plane. The longitudinal magnetoresistance for the three H-ZnO samples measured up to 8 T at 10 K and 250 K is shown in Fig. 4. The magnetoresistance is defined as  $[[R(H) - R(0)]/R(0)]$  where  $R(H)$  and  $R(0)$  are the resistances with and without an applied magnetic field, respectively.

All samples show a negative magnetoresistance at all temperatures and magnetic fields applied parallel to the main plane of the samples. The negative magnetoresistance has been observed in several other ZnO systems that show some kind of magnetic order[36, 37].

Figure 5 shows the temperature dependence of the magnetoresistance for the H-1 sample. Similar temperature dependent magnetoresistance is observed for the other two samples. It is clear from Fig. 5 that the magnetoresistance of H-ZnO decreases in general with temperature. However, its field curvature at  $T \sim 50$  K changes and from 50 K to 75 K the magnetoresistance increases with temperature. The decrease in the magnetoresistance with temperature is expected because the magnetization at saturation of these samples also decreases

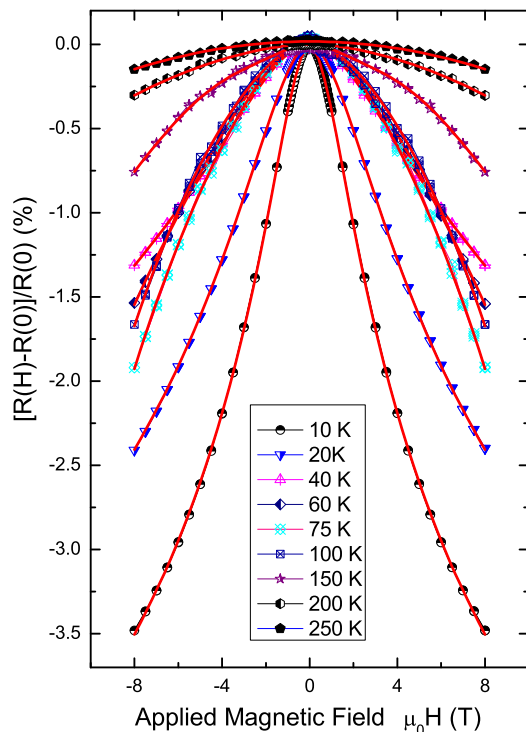


FIG. 5: Magnetoresistance of sample H-1 (the other two samples show a similar dependence) as a function of applied magnetic field measured at several temperatures. The magnetoresistance shows a negative temperature dependence but with an anomaly around 50 K. The solid (red) lines through the data points are fits to Eq. (4).

with temperature, see Fig. 1. As we have observed in the carrier concentration, the anomalous behavior in the magnetoresistance around 50 K might be related to the change of the main contribution to the resistance. Taking into account that the main contribution to the magnetic signal comes from the 20 nm surface contribution, the variable range hopping part and the magnetic semi-conducting part might have a common interface, which shows magnetic order and contributes to the magnetoresistance at low temperatures.

To elucidate our experimental results for the magnetoresistance we use a model proposed by Khosla and Fischer[38] that combines negative and positive magnetoresistances in semiconductors taking into account a third-order expansion of the  $s-d$  exchange Hamiltonian. The semiempirical formula is:

$$\frac{\Delta\rho}{\rho_0} = -a^2 \ln(1 + b^2 B^2) + \frac{c^2 B^2}{1 + d^2 B^2}, \quad (4)$$

where  $c$  and  $d$  depend on the conductivity and the carrier mobility, respectively. We will consider these as free parameters, and

$$a^2 = A_1 J \rho_F [S(S+1) + \langle M^2 \rangle], \quad (5)$$

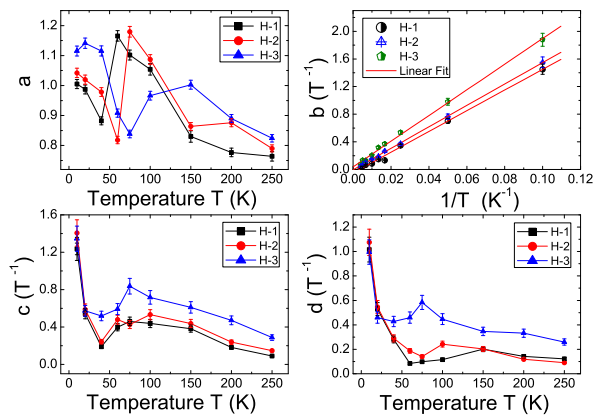


FIG. 6: Temperature dependence of the fitting parameters  $a$ ,  $b$ ,  $c$  and  $d$  of three H-ZnO samples.

$$b^2 = \left[ 1 + 4S^2\pi^2 \left( \frac{2J\rho_F}{g} \right)^4 \right] \frac{g^2\mu^2}{(\alpha kT)^2}, \quad (6)$$

where  $\mu$  is the mobility,  $g$  is the Landé  $g$ -factor,  $\alpha$  is a numerical constant. The fitting parameters  $a$  and  $b$  in Eq. (4) depend on several factors such as a spin scattering amplitude  $A_1$ , the exchange integral  $J$ , the density of states at the Fermi energy  $\rho_F$ , the spin of the localized magnetic moments  $S$  and the average magnetization square  $\langle M^2 \rangle$ . The negative first term in Eq. (4) is attributed to a spin dependent scattering in third order  $s-d$  exchange Hamiltonian while the positive part (second term in the expression of Eq. (4)) takes into account field induced changes due to the two,  $s$  and  $d$ , conduction bands with different conductivities.

The fits of the experimental data to Eq. (4) are shown in Fig. 5. The data can be well fitted with this model at all measured temperatures. All four fitting parameters show different temperature dependence (see Fig.6). Note that the positive magnetoresistance in our samples is compensated by the large negative magnetoresistance contribution. Therefore, the uncertainty of the parameters  $c$  and  $d$  is rather large because they are not independent of the fitting procedure. Therefore, we concentrate on the negative scattering contributions  $a$  and  $b$ . The fitting parameter  $b$  for the three H-ZnO samples are plotted as a function of inverse temperature in Fig. 6. The parameter  $b$  shows a linear dependence in good agreement with theory. We found that the parameter  $a$  is almost temperature independent and increases with H-concentration in the temperature range  $50 \text{ K} \leq T \leq 100 \text{ K}$  indicating that the sample with higher H-concentration (H-3) is more magnetic, in agreement with the SQUID data shown in Fig. 1.

Parameters  $a$  and  $b$  defined in Eq. (5) and Eq. (6) respectively, are used in order to obtain the values of  $J\rho_F$  and  $A_1$ . The values of  $J\rho_F$  and  $A_1$  obtained from the experimental data are 0.56 and 0.14 for  $S = 1/2$  and  $\mu$

= 36 cm<sup>2</sup>/V.s at 10 K, respectively. The values of  $J\rho_F$  and  $A_1$  for  $S = 3/2$  are 0.33 and 0.12, respectively. The value of  $J\rho_F = 0.33$  for  $S = 3/2$  in H-ZnO is similar to the one obtained in CdS system  $J\rho_F = 0.4$  [38]. These results strongly suggest the contribution of  $s-d$  interaction in the H-ZnO system.

### E. Anisotropic Magnetoresistance

There are two other magnetotransport effects, which are observed in our H-ZnO crystals and are worth mentioning. One of them is the anisotropic magnetoresistance (AMR) effect. This effect represents the change in the resistance of a ferromagnetic material with the angle between the input current and applied field in plane. It is commonly associated with the presence of a spin splitting of the electronic band at the Fermi level and a finite spin-orbit ( $L-S$ ) coupling. The AMR arises in second order in the  $L-S$  coupling, in contrast to the magnetocrystalline anisotropy. In ferromagnetic materials with  $s-$  and  $d-$ bands the AMR is understood arguing that the spin-orbit scattering increases the resistance by allowing a spin-flip and through this the occupation of free  $d-$ states in the corresponding spin dependent band. In general it is expected that the resistance is larger when the applied field is parallel to the current. We define the AMR amplitude as

$$\Delta R/R_{\text{avg}} = \frac{|R(H_{\parallel}) - R(H_{\perp})|}{(R(H_{\parallel}) + R(H_{\perp}))/2}. \quad (7)$$

For polycrystalline ferromagnetic samples the change of the resistance due to the AMR has the following angle dependence:

$$\frac{\Delta R}{R(H=0)} = A \cos^2 \theta, \quad (8)$$

where  $\theta$  is the angle between the current  $I$  and the applied field or magnetization direction (in saturation) and  $A$  is a constant that depends on the density of  $d$ -states at the Fermi level, on the magnetization as well as on the sample quality.

Figure 7 shows the field dependence of the magnetoresistance for  $\theta = 0^\circ$  and  $90^\circ$  at 10 K for the three H-ZnO samples. The angle  $\theta$  is the angle between the applied current and the magnetic field. We observe a clear AMR effect in the three H-ZnO samples. We note that the AMR effect was already measured in ZnO but doped with Co[39]. Our results show clearly that a fundamental property of ferromagnetic materials as the AMR can also be obtained by DIM in an oxide. The AMR effect in H-ZnO single crystals increases with H-concentration, see Fig. 7.

However, for ferromagnetic single crystalline systems some influence from the lattice anisotropy can be expected in the AMR and in this case the angular-dependent magnetoresistance is described by a Fourier

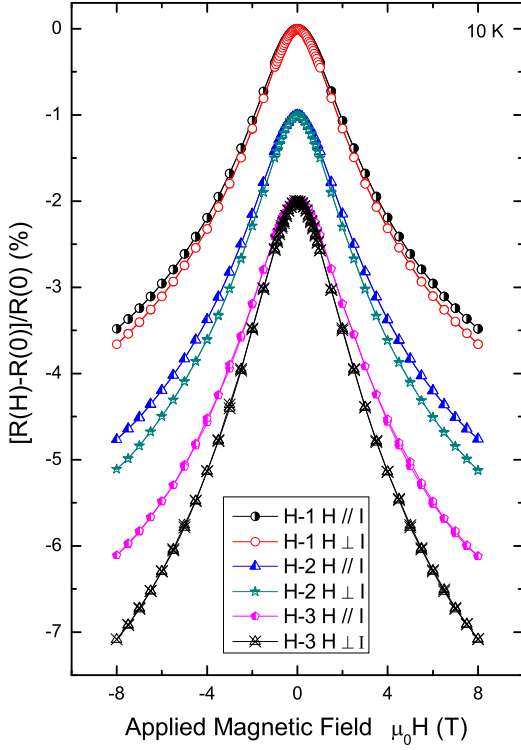


FIG. 7: Magnetoresistance of the H-ZnO samples at 10 K for two configurations of angles between current and the applied magnetic field. For clarity the data curves of the samples H-2 and H-3 are shifted by a constant value.

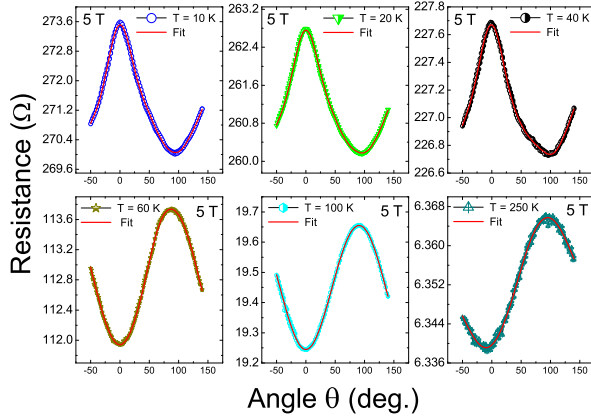


FIG. 8: Angular magnetoresistance of sample H-1 at a constant field of 5 T at several temperatures. The red solid lines are the fits to experimental data following Eq. (9).

series of  $\cos(n\theta)$  and  $\sin(n\theta)$  as

$$\frac{\Delta R}{R(H=0)} = \sum_{n=1}^{n=\infty} s_n \sin(n\theta) + \sum_{n=1}^{n=\infty} c_n \cos(n\theta), \quad (9)$$

where the coefficients  $s_n$  and  $c_n$  are related to the Hall and magnetoresistance contributions in the system.

In order to study the AMR in more detail, we measured the angular magnetoresistance at a constant field of 5 T at several temperatures, see Fig. 8. The variation of the angle between the magnetic field and the current ranges from  $-50^\circ$  to  $140^\circ$ . This range of angle is necessary because we expect a  $180^\circ$  periodicity. There are several distinct features in the experimental data shown in Fig. 8. (a) At  $T < 50$  K the AMR is higher at  $\theta = 0^\circ$  (field and current parallel to each other) than at  $\theta = 90^\circ$ , in agreement with the usual behavior. (b) At temperatures  $T > 50$  K the AMR changes sign (or it shows a  $90^\circ$  shift in the angle dependence), see Fig. 8. (c) Figure 9 shows the AMR amplitude, see Eq.(7), as a function of temperature for the three samples. There is a clear anomalous increase with temperature between 50 K and 100 K, in spite of the fact the the magnetization at saturation decreases monotonously in all the temperature range according to the SQUID measurements (not shown). Note that the magnitude of the AMR in our H-ZnO samples at 250 K is  $\sim 0.4\%$ , a value comparable to the AMR observed in, e.g., Co films[40] or Co:Cu multilayered nanowires[41]. (d) The measured angle dependence does not follow Eq. (8) applicable for polycrystalline materials and indicates that the magnetic contribution in our H-ZnO single crystals comes from a single crystalline phase after H-plasma treatment. The AMR curves obtained for all three H-ZnO samples are fitted by Eq. (9) and the results of these fits are shown in Fig. 8 as (red) solid lines. The experimental data can be fitted quite well at all temperatures after expanding Eq. (9) up to eighth order. The coefficients  $s_n$  and  $c_n$  are related to the antisymmetric (Hall) and symmetric (magnetoresistance) contributions of the sample. The values of the coefficients  $s_n$  obtained from the fits are negligibly small and therefore only the coefficients  $c_n$  are shown in Fig. 10. The major contributions to the AMR come from the terms with  $n = 2, 4, 6$  and  $8$  indicating that the action of the Lorentz force on the mobile charges is not the source for the observed AMR in H-ZnO samples.

As shown for the system ZnO-Cu with oxygen vacancies [42], however, the influence of hydrogen cannot rule out the Zn- $d$  contribution to the magnetic order as well as from the oxygen  $p$ -states. X-ray magnetic circular dichroism measurements are necessary to obtain the required information on the elements (and bands) contributions to the observed magnetic order. In particular the origin of the clear anomalous behavior at  $50 \text{ K} \lesssim T \lesssim 100 \text{ K}$  with the unexpected change of sign of the AMR effect (factor C2, see Fig.10) requires further studies that go beyond a magnetotransport characterization. We note, however, that a change of sign of the AMR (and the thermopower  $S$ ) at  $T \sim 50 \text{ K}$  has been observed for particular field directions in  $\text{U}_3\text{As}_4$  and  $\text{U}_3\text{P}_4$  ferromagnetic single crystals [43]. The author interpreted the abrupt change and sign inversion of AMR (and  $S$ ) in the frame of spin-orbit coupling (SOC) and a large sensitivity in energy of the spin density of states at the Fermi-level due to a spontaneous trigonal distortion in magnetically ordered state.

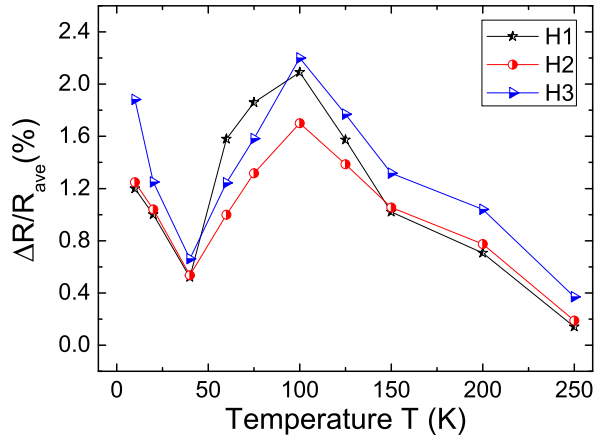


FIG. 9: Temperature dependence of the absolute value of the AMR defined in Eq. (7), for the three H-ZnO samples. Note that actually the AMR changes sign at  $T \simeq 50$  K.

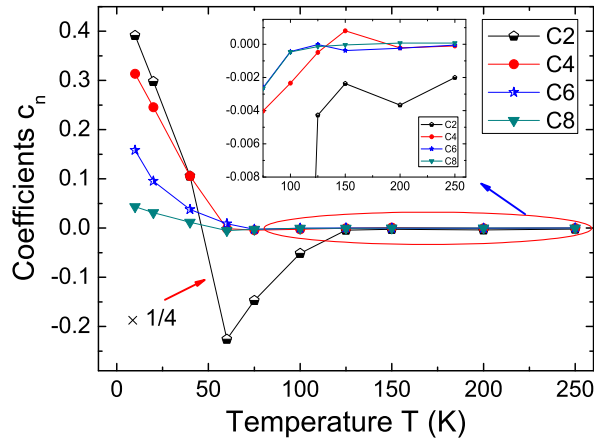


FIG. 10: Fitting coefficient  $c_n$  as a function of temperature obtained from the fits to Eq. (9) to the experimental data shown in Fig. 8. The values of the coefficient  $c_2$  are divided by 4 to include them for clarity with the other coefficients. Note that it changes sign at  $\sim 50$  K.

### F. Anomalous Hall Effect

The anomalous Hall effect (AHE) was reported in magnetic-ion doped ZnO systems in the past[44–46] but not yet in an (magnetic-ion) un-doped ZnO systems and at room temperature. The Hall resistance in ferromagnetic materials consists of two contributions which are the ordinary Hall resistance (due to Lorentz force) and the anomalous Hall resistance (due to an asymmetric scattering in the presence of magnetic order) and can be expressed by the following equation

$$R_{\text{Hall}} = R_H(H) + R_{\text{AHE}}(M), \quad (10)$$

where  $R_H$  and the  $R_{\text{AHE}}$  are the ordinary and anomalous Hall resistances and  $M$  is the magnetization. The

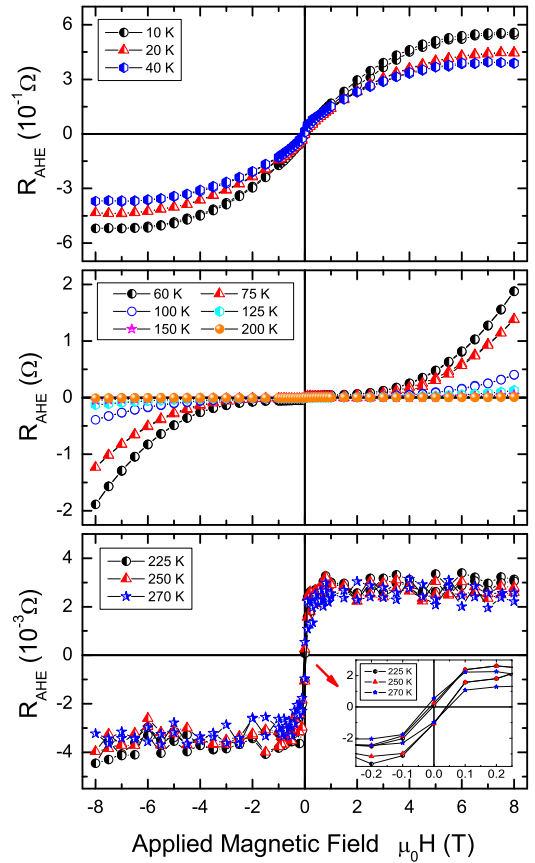


FIG. 11: Anomalous Hall resistance of the H-2 sample as a function of a magnetic field at several temperatures. The linear background from the conventional Hall effect was subtracted from the measured curves. Note that AHE shows an anomalous change of field curvature above 50 K and it is nearly temperature independent above 225 K.

dominant feature of the Hall data in our H-ZnO samples is a linear dependence of  $R_{\text{Hall}}$  with magnetic field with a negative slope due to the ordinary contribution  $R_H$ . After subtracting  $R_H(H)$  from the measured data, an anomalous Hall effect contribution is obtained for all three H-ZnO samples, as shown in Fig. 11 for sample H-2. Clear  $s$ -like loops with very weak hysteresis are observed in  $R_{\text{AHE}}(H)$  up to 300 K. The shape of the loops at temperatures  $T < 50$  K indicates that the hydrogen related paramagnetic centers dominate, in agreement with SQUID results, see Fig. 1(a). At intermediate temperatures  $50 \lesssim T \lesssim 150$  K the behavior of  $R_{\text{AHE}}(H)$  is anomalous in the sense that it has a different field curvature without saturation at large fields. Note that in the same temperature range the carrier concentration, magnetoresistance and anisotropic magnetoresistance behave also anomalously. At temperatures above 150 K the  $R_{\text{AHE}}(H)$  curves follow the expected behavior for a ferromagnet, see Fig. 11.

In order to further investigate whether the anomalous Hall effect is mainly affected by the magnetization



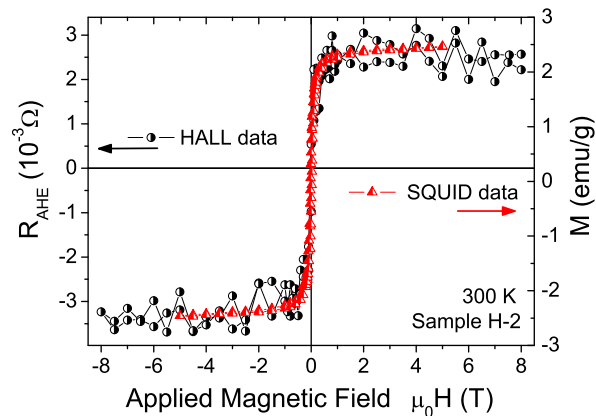


FIG. 12: A comparison of the SQUID and the anomalous Hall resistance data at 300 K.

response of the samples we compared the SQUID and  $R_{AHE}(H)$  results. Figure 12 shows the  $M(H)$  and  $R_{AHE}(H)$  loops at 300 K. Both curves are very similar, which indicate that the AHE originates from the intrinsic ferromagnetism of the H-ZnO samples.

#### IV. CONCLUSION

We have studied the magnetic and magnetotransport properties of H-implanted ZnO single crystals with different hydrogen concentrations in the atomic percent range. Clear ferromagnetic-like loops were observed in all three H-ZnO samples at room temperature with a magnetization at saturation up to 4 emu/g. The Hall measurements confirmed the n-type transport mechanism in H-ZnO. We observed a negative magnetoresistance in all

crystals and in the available temperature and magnetic field range. The magnitude of the magnetoresistance increases with H-concentration. We observed the anomalous Hall effect and anisotropic magnetoresistance in the H-ZnO single crystals. The magnitude of anisotropic magnetoresistance was found to be 0.4 % at 250 K, a value comparable to polycrystalline cobalt. The anomalous Hall effect data showed a quantitative agreement to the SQUID data for all three H-ZnO single crystals, a fact that excludes impurities as the origin of the observed ferromagnetism. The observation of anisotropic magnetoresistance up to room temperature strongly suggests the presence of a spin-split band with a non-zero spin-orbit coupling in H-ZnO single crystals. At temperatures below 100 K, anomalous behaviors in the magnetoresistance, anisotropic magnetoresistance, and carrier density were observed that are apparently related to the change of the main contribution to the measured resistance, i.e. from semiconducting to VRH-like transport. We believe that our findings would be useful for further understanding of defect induced magnetism in ZnO as well as other oxide systems and could be the starting point towards an efficient and reproducible way of inducing ferromagnetism in ZnO systems.

#### Acknowledgments

We gratefully acknowledge Prof. J. Weber and Dr. E. Lavrov from the Technical University of Dresden for the support in preparing the ZnO crystals in their laboratory. We thank Dr. M. Ziese for fruitful discussions. This work was supported by the DFG within the Collaborative Research Center (SFB 762) “Functionality of Oxide Interfaces”.

- 
- [1] P. Esquinazi, D. Spemann, R. Höhne, A. Setzer, K.-H. Han, and T. Butz, *Phys. Rev. Lett.* **91**, 227201 (2003).  
 [2] H. Ohldag, P. Esquinazi, E. Arenholz, D. Spemann, M. Rothermel, A. Setzer, and T. Butz, *New Journal of Physics* **12**, 123012 (2010).  
 [3] H. Pan, J. B. Yi, L. Shen, R. Q. Wu, J. H. Yang, J. Y. Lin, Y. P. Feng, J. Ding, L. H. Van, and J. H. Yin, *Phys. Rev. Lett.* **99**, 127201 (2007).  
 [4] V. Bhosle and J. Narayan, *Appl. Phys. Lett.* **93**, 021912 (2008).  
 [5] K. Potzger, S. Zhou, J. Grenzer, M. Helm, and J. Fassbender, *Appl. Phys. Lett.* **92**, 182504 (2008).  
 [6] Q. Xu, H. Schmidt, S. Zhou, K. Potzger, M. Helm, H. Hochmuth, M. Lorenz, A. Setzer, P. Esquinazi, C. Meinecke, et al., *Appl. Phys. Lett.* **92**, 082508 (2008).  
 [7] M. Khalid, M. Ziese, A. Setzer, P. Esquinazi, M. Lorenz, H. Hochmuth, M. Grundmann, D. Spemann, T. Butz, G. Brauer, et al., *Phys. Rev. B* **80**, 035331 (2009).  
 [8] M. Khalid, A. Setzer, M. Ziese, P. Esquinazi, D. Spemann, A. Pöpl, and E. Goering, *Phys. Rev. B* **81**, 214414 (2010).  
 [9] M. Venkatesan, C. B. Fitzgerald, and J. M. D. Coey, *Nature* **430**, 630 (2004).  
 [10] S. Duhalde, M. F. Vignolo, F. Golmar, C. Chilotte, C. E. R. Torres, L. A. Errico, A. F. Cabrera, M. Renteria, F. H. Sanchez, and M. Weissmann, *Phys. Rev. B* **72**, 161313 (2005).  
 [11] N. H. Hong, J. Sakai, N. Poirot, and V. Brizé, *Phys. Rev. B* **73**, 132404 (2006).  
 [12] K. Potzger, J. Osten, A. A. Levin, A. Shalimov, G. Talut, H. Reuther, S. Arpaci, D. Bürger, H. Schmidt, T. Nestler, et al., *J. Magn. Magn. Mat.* **323**, 1551 (2011).  
 [13] I. S. Elfimov, A. Rusydi, S. I. Csiszar, Z. Hu, H. H. Hsieh, H.-J. Lin, C. T. Chen, R. Liang, and G. A. Sawatzky, *Phys. Rev. Lett.* **98**, 137202 (2007).  
 [14] Y. Liu, G. Wang, S. Wang, J. Yang, L. Chen, X. Qin, B. Song, B. Wang, and X. Chen, *Phys. Rev. Lett.* **106**, 087205 (2011).  
 [15] M. Stoneham, *J. Phys.: Condens. Matter* **22**, 074211 (2010).

- [16] O. Volnianska and P. Boguslawski, *J. Phys.: Condens. Matter* **22**, 073202 (2010).
- [17] O. V. Yazzev, *Rep. Prog. Phys.* **73**, 056501 (2010).
- [18] A. N. Andriotis, R. M. Sheetz, and M. Menon, *J. Phys.: Condens. Matter* **22**, 334210 (2010).
- [19] T. Heng, D.C.Qi, T. Berlijn, J.B.Yi, K. Yang, Y. Dai, Y. Feng, I. Santoso, C. Sanchez-Hanke, X. Gao, et al., *Phys. Rev. Lett.* **105**, 207201 (2010).
- [20] R. Singhal, A. Samariya, S. Kumar, Y. Xing, U. Deshpande, T. Shripathi, and E. Baggio-Saitovitch, *J. of Magnetism and Magnetic Materials* **322**, 2187 (2010).
- [21] M. Assadi, Y. Zhang, and S. Li, *J. Phys: Condens. Matter* **22**, 156001 (2010).
- [22] N. Sanchez, S. Gallego, J. Cerdá, and M. C. Muñoz, *Phys. Rev. B* **81**, 115301 (2010).
- [23] E. Liu and J. Jiang, *J. Phys. Chem. C* **113**, 16116 (2009).
- [24] M. Khalid, P. Esquinazi, D. Spemann, W. Anwand, and G. Brauer, *N. J. of Phys.* **13**, 063017 (2011).
- [25] J. Zieger, J. Biersack, and U. Littmark, *The stopping and range of ions in solids* (Pergamon, New York, 1985), vol. 1.
- [26] W. Lanford, *Handbook of Modern Ion Beam Materials Analysis* (Materials Research Society, Pittsburgh/PA, 1995), p. 193.
- [27] W. Anwand, G. Brauer, T. Cowan, D. Grambole, W. Skorupa, J. Cizek, J. Kuriplach, I. Prochazka, W. Egger, and P. Sperr, *Phys. Status Solidi A* **207**, 2415 (2010).
- [28] D. G. Thomas and J. J. Lander, *J. Chem. Phys.* **22**, 83 (1954).
- [29] J. Barzola-Quiquia, P. Esquinazi, M. Villafuerte, S. P. Heluani, A. Poppl, and K. Eisinger, *J. of Appl. Phys.* **108**, 073530 (2010).
- [30] C. Hung and J. Gliessmann, *Phys. Rev.* **96**, 1226 (1954).
- [31] H. Nishimura, *Phys. Rev.* **138**, A815 (1965).
- [32] B. Shklovskii and A. Efros, *Electronic properties of doped semiconductors* (New York: Springer, 1984).
- [33] S. Majumdar and P. Banerji, *J. of Appl. Phys.* **107**, 063702 (2010).
- [34] T. Yamada, A. Miyake, S. Kishimoto, H. Makino, N. Yamamoto, and T. Yamamoto, *Appl. Phys. Lett.* **91**, 051915 (2007).
- [35] N. W. Ashcroft and N. D. Mermin, *Solid State Physics* (Holt-Saunders International Editions, 1981, page 240 ff.).
- [36] A. Kumar, J.-M. Poumirol, W. Escoffier, . Goiran, B. Raquet, and J. C. Pivin, *J. Phys.: Condens. Matter* **22**, 436004 (2010).
- [37] S. shen Yan, C. Ren, X. Wang, Y. Xin, Z. X. Zhou, L. M. Mei, M. J. Ren, Y. X. Chen, Y. H. Liu, and H. Garmestani, *Appl. Phys. Lett.* **84**, 2376 (2004).
- [38] R. Khosla and J. Fischer, *Phys. Rev. B* **2**, 4084 (1970).
- [39] K. W. Lee and C. E. Lee, *Phys. Rev. Lett.* **97**, 137206 (2006).
- [40] J. Barzola-Quiquia, W. Böhlmann, P. Esquinazi, A. Schadewitz, A. Ballestar, S. Dusari, L. Schultze-Nobre, and B. Kersting, *Appl. Phys. Lett.* **98**, 192511 (2011).
- [41] L. Tan, P. McGary, and B. Stadler, *J. of Appl. Phys.* **103**, 07B504 (2008).
- [42] T. S. Heng, D.-C. Qi, T. Berlijn, J. B. Yi, K. S. Yang, Y. Dai, Y. P. Feng, I. Santoso, C. Sánchez-Hanke, X. Y. Gao, et al., *Phys. Rev. Lett.* **105**, 207201 (2010).
- [43] P. Wiśniewski, *Appl. Phys. Lett.* **90**, 192106 (2007).
- [44] H. S. Hsu, C. P. Lin, H. Chou, and J. C. A. Huang, *Appl. Phys. Lett.* **93**, 142507 (2008).
- [45] Z. Yang, M. Biasini, W. P. Beyermann, M. B. Katz, O. K. Ezekoye, X. Q. Pan, Y. Pu, J. Shi, Z. Zuo, and J. L. Liu, *Appl. Phys. Lett.* **104**, 113712 (2008).
- [46] Q. Xu, L. Hartmann, H. Schmidt, H. Hochmuth, M. Lorenz, R. Schmidt-Grund, C. Sturm, D. Spemann, M. Grundmann, and Y. Liu, *J. of Appl. Phys.* **101**, 063918 (2007).